Anat Embryol (2001) 204:267–282

REVIEW ARTICLE

Arthur W. Toga · Paul M. Thompson
Michael S. Mega · Katherine L. Narr
Rebecca E. Blanton

Probabilistic approaches for atlasing normal and disease-specific brain variability

Accepted: 9 May 2001

Abstract The extreme variability in the structural conformation of the human brain poses significant challenges for the creation of population-based atlases. The ability to statistically and visually compare and contrast brain image data from multiple individuals is essential to understanding normal variability within a particular population as well as differentiating normal from diseased populations. This paper introduces the application of probabilistic atlases that describe specific subpopulations, measures their variability and characterizes the structural differences between them. Utilizing data from structural MRI, we have built atlases with defined coordinate systems creating a framework for mapping data from functional, histological and other studies of the same population. This paper describes the basic approach and a brief description of the underlying mathematical constructs that enable the calculation of probabilistic atlases and examples of their results from several different normal and diseased populations.

Keywords Brain imaging · Probabilistic brain atlases · Normal and disease-specific brain variability

Introduction

An atlas of the brain allows us to define its spatial characteristics. Where is a given structure; what is its shape and how do we refer to it? How similar or different is this brain compared to normals? An atlas allows us to answer these and related questions quantitatively and visually.

A.W. Toga (✉) · P.M. Thompson · K.L. Narr · R.E. Blanton
Rm. 4238, Reed Neurological Research Center,
Laboratory of Neuro Imaging, Department of Neurology,
UCLA School of Medicine, 710 Westwood Plaza,
Los Angeles, CA 90095-1769, USA
e-mail: toga@loni.ucla.edu
Tel.: +1-310-206-2101, Fax: +1-310-206-5518

M.S. Mega
Alzheimer's Disease Center, Department of Neurology,
UCLA School of Medicine, Los Angeles, California, USA

Comprehensive maps of brain structure have been derived, at a variety of spatial scales, from 3D tomographic images (Damasio 1995), anatomic specimens (Talairach and Szikla 1967; Talairach and Tournoux 1988; Ono et al. 1990; Duvernoy 1991) and a variety of histologic preparations that reveal regional cytoarchitecture (Brodmann 1909), myelination patterns (Smith 1907), protein densities and mRNA distributions. Most early atlases of the human brain, and other species (Paxinos and Watson 1986), were derived from one, or at best a few, individual post mortem specimens (Brodmann 1909; Schaltenbrand and Bailey 1959; Schaltenbrand and Wahren 1977; Talairach and Szikla 1967; Matsui and Hirano 1978; Talairach and Tournoux 1988; Ono et al. 1990). Such atlases take the form of anatomical references or represent a particular feature of the brain (Van Buren and Maccubin 1962; Van Buren and Borke 1972), such as a specific neurochemical distribution (Mansour et al. 1995) or the cellular architecture of the cerebral cortex (Brodmann 1909). Other brain atlases map function, quantified by positron emission tomography (PET; Minoshima et al. 1994), functional MRI (Le Bihan 1996) or electrophysiology (Avoli et al. 1991; Palovcik et al. 1992). Maps also have been developed to represent neuronal connectivity and circuitry (Van Essen and Maunsell 1983) based on compilations of empirical evidence (Brodmann 1909; Berger 1929; Penfield and Boldrey 1937).

Beyond the anatomic atlases based on post mortem and histologic material mentioned above, the application of magnetic resonance to acquire detailed descriptions of anatomy in vivo is a driving force in brain mapping research. MRI data have the advantage of intrinsic three-axis registration and spatial coordinates (Damasio 1995), but have relatively low resolution and lack anatomic contrast in important subregions. Even high-resolution MR atlases, with up to 100–150 slices, a section thickness of 2 mm, and 256^2 pixel imaging planes (Evans et al. 1991; Lehmann et al. 1991) still result in resolutions lower than the complexity of many neuroanatomic structures. However, advances in the technology contin-

ue to push improvements in spatial and contrast resolution. A recent innovation in the collection of atlas quality MRI involves the averaging of multiple co-registered scans (N=27) from a single subject to overcome the lack of contrast and relatively poor signal to noise (Holmes et al. 1998).

Unfortunately each of the brain maps contained in these atlases (post mortem and in vivo) has a different spatial scale and resolution, emphasizes different structural or functional characteristics, and is inherently incompatible with the others. Each mapping strategy clearly has its place within a collective effort to map the brain, but unless certain integrative approaches are implemented (including spatial normalization), these brain maps will remain as individual and independent efforts, and the correlative potential of the many diverse mapping approaches will be underexploited.

A crucial element for integrating multiple brain maps is the construction of averages, templates and models to describe how the brain and its component parts are organized. Design of appropriate reference systems for brain data presents considerable challenges, since these systems must capture how brain structure and function vary in large populations, across age and gender, in different disease states, across imaging modalities, and even across species.

Population-based brain atlases (the focus of this paper) offer a powerful framework to synthesize the results of disparate imaging studies. These atlases use novel analytical tools to fuse data across subjects, modalities, and time. They detect group-specific features not apparent in individual scans. Population based atlases can be stratified into subpopulations to reflect a particular (clinical) subgroup (Toga and Mazziotta, 1996).

Imaging algorithms are also significantly improving the flexibility of digital brain atlases. *Deformable brain atlases* are adaptable in that they can be individualized to reflect the anatomy of new subjects, and *probabilistic atlases* retain information on cross-subject variations in brain structure and function. These atlases are powerful new tools with broad clinical and research applications (Roland and Zilles 1994; Kikinis et al. 1996; Toga and Thompson 1998). Despite the significant challenges in expanding the atlas concept to the time dimension, dynamic brain atlases are beginning to include probabilistic information on growth rates that may assist research into pediatric disorders (Thompson and Toga 1999).

Anatomic variations severely hamper the integration and comparison of data across subjects and groups (Meltzer and Frost 1994; Woods 1996). Motivated by the need to standardize data across subjects, analytic methods were developed to remove size and shape differences that distinguish one brain from another (Talairach and Tournoux 1988). Spatially transforming individual brain maps onto a 3D digital brain atlas, removes subject-specific shape variations, and allows subsequent comparison of brain structure or function between individuals (Christensen et al. 1993; Ashburner et al. 1997). Conversely, *deformable brain atlases* are based on the idea that a digital brain atlas can be elastically deformed to fit a new subject's anatomy (Evans et al. 1991; Gee et al. 1993; Christensen et al. 1993; Sandor and Leahy 1995; Rizzo et al. 1995; Toga and Thompson 1997; Haller et al. 1997). High-dimensional brain *warping* algorithms (Christensen et al. 1993; 1996; Collins et al. 1994a; Thirion 1995; Rabbitt et al. 1995; Warfield et al. 1995; Davatzikos 1996; Thompson and Toga 1996; Bro-Nielsen and Gramkow 1996; Gee and Bajscy 1998; Grenander and Miller 1998) effect the transfer of 3D maps of structure, function and other descriptions such as information on cytoarchitecture, histologic and neurochemical content (Mega et al. 1997) onto the scan of any subject.

The coordinate system used to equate brain topology with an index must include carefully selected features common to all brains. Further, these features must be readily identifiable and sufficiently distributed anatomically to avoid bias. Once defined, rigorous systems for matching, or spatially normalizing a brain to this coordinate system must be utilized. This allows individual data to be transformed to match the space occupied by the atlas. In the Talairach stereotaxic system (Talairach and Szikla 1967; Talairach and Tournoux 1988), piecewise affine transformations are applied to 12 rectangular regions of brain, defined by vectors from the anterior and posterior commissures to the extrema of the cortex. These transformations re-position the anterior commissure of the subject's scan at the origin of the 3D coordinate space, vertically align the interhemispheric plane, and horizontally orient the line connecting the two commissures. Each point in the incoming brain image, after it is registered into the atlas space, is labeled by an (x, y, z) address indexed to the atlas brain. Although originally developed to help interpret brain stem and ventricular studies acquired using pneumoencephalography (Talairach and Szikla 1967), the Talairach stereotaxic system rapidly became an international standard for reporting functional activation sites in PET studies, allowing researchers to compare and contrast results from different laboratories (Fox et al. 1985, 1988; Friston et al. 1989, 1991).

Perhaps surprisingly, few atlases of neuropathology use a standardized 3-dimensional coordinate system to integrate data across patients, techniques, and acquisitions. Atlases with a well-defined coordinate space (Evans et al. 1992; Friston et al. 1995; Drury and van Essen 1997), together with algorithms to align data with them (Toga 1998), have enabled the pooling of brain mapping data from multiple subjects and sources, including large patient populations. Automated algorithms can then capitalize on atlas descriptions of anatomical variance to guide image segmentation (Le Goualher et al. 1999; Pitiot et al. 1999), tissue classification (Zijdenbos and Dawant 1994), functional image analysis (Dinov et al. 1999), and pathology detection (Thompson et al. 1997, 2000).

This paper not only discusses the construction and application of normal population-based atlases but includes descriptions of the concept of disease-specific atlases, designed to reflect the unique anatomy and physiology

of a particular clinical subpopulation (Thompson et al. 1997, 1998, 2000c; Mega et al. 1997, 1998, 1999; Narr et al. 1999; 2000). Based on well-characterized patient groups, these atlases contain composite maps and visualizations of structural variability, asymmetry and group-specific differences. This quantitative framework can be used to recognize anomalies and label structures in new patients. Because they retain information on group anatomical variability, disease-specific atlases are a type of probabilistic atlas specialized to represent a particular clinical group. The resulting atlases can identify patterns of altered structure or function, and can guide algorithms for knowledge-based image analysis (Collins et al. 1994b; Pitiot et al. 1999; Dinov et al. 1999).

Modeling strategies currently used to represent brain data have been motivated by the need to extract and analyze the complex shape of anatomical structures, for high-resolution visualization and quantitative comparisons. Standard 3D modeling approaches can be used to examine often-studied structures such as the ventricles, and can provide a framework for mapping variation within and between different populations. An underlying 3D coordinate system is central to all atlas systems, since it supports the linkage of structure models and associated image data with spatially-indexed neuroanatomic labels, preserving spatial information and adding anatomical knowledge.

We present data from several on-going projects, whose goal is to create disease-specific atlases of the brain in Alzheimer's disease, schizophrenia, and several neurodevelopmental disorders. Pathological change can be tracked over time, and disease-specific features resolved. Rather than simply fusing information from multiple subjects and sources, we describe strategies used to resolve group-specific features not apparent in individual scans.

Methods

To create atlases that contain detailed representations of anatomy, rather than utilizing intensity criteria to define structures, we have developed model-driven algorithms that deform them to match the anatomy of new subjects (Thompson et al. 2000c, 1996, 1997, 2000a; Toga and Thompson 1997). Anatomic models provide an explicit geometry for individual structures in each scan, such as landmark points, curves or surfaces. Because the digital models reside in the same stereotaxic space as the atlas data, surface and volume models stored as lists of vector coordinates are amenable to digital transformation, as well as geometric and statistical measurement (Thompson et al. 1996a, 1998, 2000b; Mega et al. 1998; Zhou et al. 1999; Narr et al. 2000). The underlying 3D coordinate system is central to all atlas systems, since it supports the linkage of structure models and associated image data with spatially-indexed neuroanatomic labels, preserving spatial information and adding anatomical knowledge (Fig. 1).

When deforming an atlas to match a patient's anatomy, mesh-based models of anatomic systems help guide the mapping of one brain to another. Anatomically driven algorithms guarantee biological as well as computational validity, generating meaningful object-to-object correspondences, especially at the cortex. In this model-based approach (Thompson and Toga 1996, 1997, 1998), systems of surfaces are first extracted from each dataset, to guide the volumetric mapping. The model surfaces include many functional, cytoarchitectonic and lobar boundaries in three dimensions. Both the surfaces and the landmark curves within them are reconfigured to match their counterparts in the target datasets exactly.

Anatomical models

Since much of the functional territory of the human cortex is buried in sulci, a generic structure is built to model them (Thompson and Toga 1996). The underlying data structure is a connected system of surface meshes, in which the individual meshes are parametric. These surfaces are 3D sheets that divide and join at curved junctions to form a connected network of models. With the help of these meshes, each patient's anatomy is modeled in sufficient detail to be sensitive to subtle differences in disease. Separate surfaces model the deep internal trajectories of features such as the parieto-occipital sulcus, the anterior and posterior calcarine sulcus, the Sylvian fissure, and the cingulate, marginal and supracallosal sulci in both hemispheres. Additional gyral boundaries are represented by parameterized curves lying in the cortical surface. The ventricular system is modeled as a closed system of 14 connected surface elements whose junctions reflect cytoarchitectonic boundaries of the adjacent tissue (Thompson and Toga 1998). Information on the meshes' spatial relations, including their surface topology (*closed* or *open*), anatomical names, mutual connections, directions of parameterization, and common 3D junctions and boundaries is stored in a hierarchical graph structure. This ensures the continuity of displacement vector fields defined at mesh junctions.

Surface parameterization

After imposing an identical regular grid structure on anatomic surfaces from different subjects, the explicit geometry can be exploited to drive and constrain correspondence maps that associate anatomic points in different subjects. Structures that can be extracted automatically in parametric form include the external cortical surface, ventricular surfaces, and several deep sulcal surfaces. Recent success of sulcal extraction approaches based on deformable surfaces (Vaillant and Davatzikos 1999) led us to combine a 3D skeletonization algorithm with deformable curve and surface governing equations to automatically produce parameterized models of cingulate, parieto-occipital, and calcarine sulci, without manual initialization (Zhou et al. 1999). Additional, manually-segmented surfaces can also be given a uniform rectilinear parameterization using algorithms described in (Thompson et al. 1996a,b), and used to drive the warping algorithm. Each resultant surface mesh is analogous in form to a uniform rectangular grid, drawn on a rubber sheet, which is subsequently stretched to match all data points. Association of points on each surface with the same mesh coordinate produces a dense correspondence vector field between surface points in different subjects; Fig. 1. This procedure is carried out under stringent conditions to ensure that landmark curves and points known to the anatomist appear in corresponding locations in each parametric grid.

Maps of the cortical parameter space

Detailed models of cortical anatomy are also created by driving a tiled, spherical mesh into the configuration of each subject's cortex (Thompson and Toga 1996; MacDonald 1998). Because these cortical models are obtained by deforming a spherical mesh, any point on the cortical surface must map to exactly one point on the sphere and vice versa. Each cortical surface is parameterized with an invertible mapping, so sulcal curves and landmarks in the folded brain surface can be reidentified in the spherical map (*cf*. Sereno et al. 1996, Fischl et al. 1999, for a similar approach). To retain relevant 3D information, cortical surface point position vectors in 3D stereotaxic space are color-coded, so that a unique color is placed at each position on the spherical map indicating the

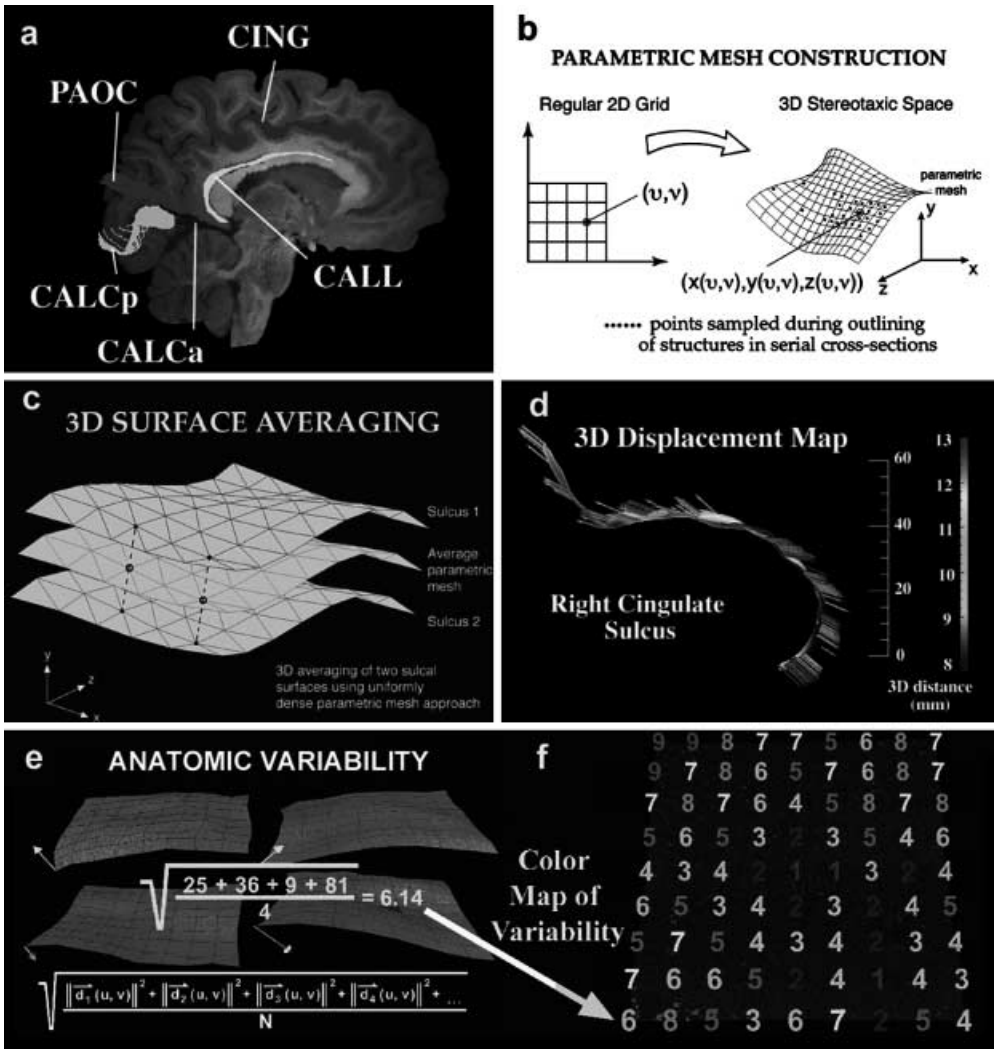

Fig. 1a–f Anatomical mesh construction and averaging. The derivation of a standard surface representation for each structure makes it easier to compare anatomical models from multiple subjects. An algorithm converts a set of digitized points on an anatomical structure boundary (e.g., deep sulci (**a**)) into a parametric grid of uniformly spaced points in a regular rectangular mesh stretched over the surface (**b**); Thompson et al. 1996). By averaging nodes with the same grid coordinates across subjects (**c**), an average surface is produced for the group. However, information on each subject's individual differences is retained as a vector-valued displacement map (**d, e**). This map indicates how that subject deviates locally from the average anatomy. The root mean square magnitude (**e**) of these deviations provides a variability measure whose values can be visualized using a color code (**f**). These maps can be stored to measure variability in different anatomic systems, including ventricular and deep sulcal (Thompson et al. 1998) surfaces. A more complex method measures cross-subject variations in gyral patterns, with a surface matching procedure that better reflects anatomical variations at the cortex. These maps can be stored to measure variability (**f**) and detect abnormalities in different anatomic systems. (Adapted from Thompson et al. 2000b)

3D position of the cortical point that maps to it. In other words, the colors represent 3D locations, and the entire set of colors forms an image on the sphere in a color image format. To find good matches between cortical regions in different subjects, we first derive a spherical map for each respective cortical surface model and then perform a matching process in the spherical parametric space. A flow field is calculated on the sphere that brings corresponding gyral and sulcal regions into the same spherical locations across subjects (Davatzikos 1996; Drury et al. 1996; Van Essen et al. 1997; Fischl et al. 1999). This warp can be set up in a variety of ways. Spherical harmonic functions are an orthonormal basis on the sphere, which means that any smooth flow on the sphere can be represented with arbitrarily high accuracy using a linear combination of these functions, so long as a sufficient number of functions is used. The resulting flow field can align structural or functional information across subjects, bringing curve and surface interfaces into exact register in the process (Thompson and Toga 1996). Alternatively, an approach based on covariant partial differential equations can be used for matching cortical surfaces (Thompson et al. 2000e). This precisely matches cortical landmarks across subjects, and creates maps that are independent of the surface metrics. The approach ensures that the way cortical structures are matched in 3D is independent of the way the surfaces are computationally represented (irrespective of their tile density and parameterizations).

Tensor maps of directional variation

Structures do not vary to the same degree in every coordinate direction (Thompson et al. 1996), and even these directional biases vary by cortical system. The principal directions of anatomic variability in a group can be shown in a *tensor map* (Thompson et al. 2000a,b). The maps have two uses. First, they make it easier to detect anomalies, which may be small in magnitude but in an un-

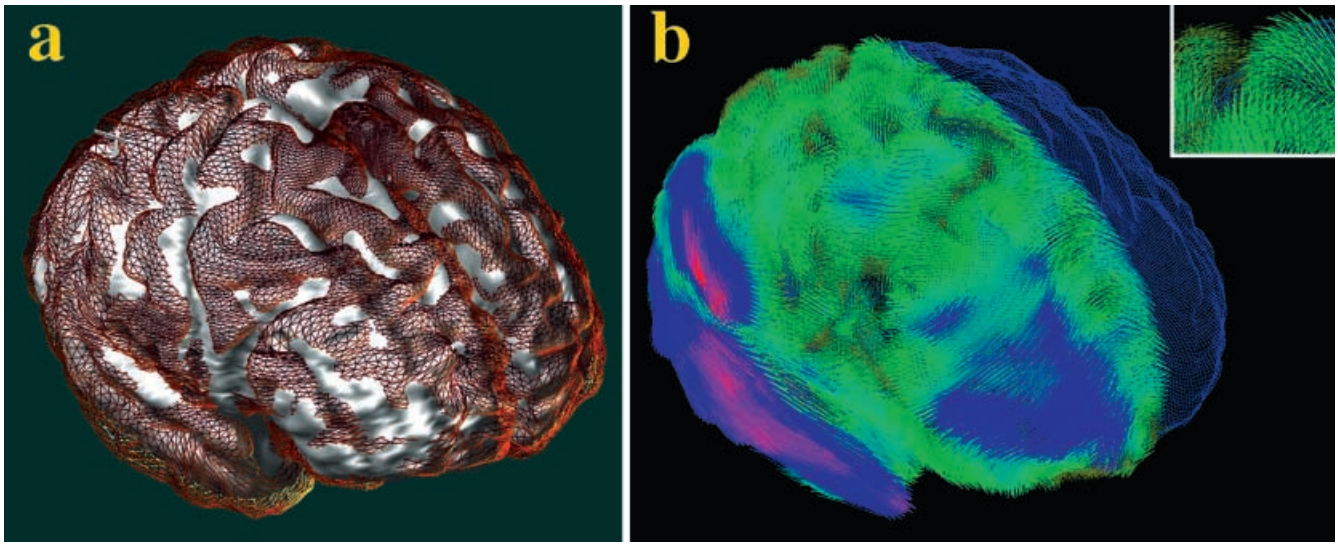

Fig. 2a, b Matching an individual's cortex to the average cortex. 3D variability patterns across the cortex are measured by driving individual cortical patterns into local correspondence with the average cortical model. **a** Shows how the anatomy of one subject (*brown surface mesh*) deviates from an average cortical model (*white*), after affine alignment of the individual data. **b** shows the deformation vector field required to reconfigure the gyral pattern of the subject into the exact configuration of the average cortex. The transformation is shown as a flow field that takes the individual's anatomy onto the right hemisphere of the average cortex (*shown as a blue surface mesh*). The largest amount of deformation is required in the temporal and parietal cortex (*pink colors, large deformation*). Details of the 3D vector deformation field ((b), *inset*) show the local complexity of the mapping. Storage of these mappings allows quantification of local anatomic variability. (Adapted from Thompson et al. 2000b)

usual direction. Second, they significantly increase the information content of Bayesian priors used for automated structure extraction and identification (Gee et al. 1993; Mangin et al. 1994; Royackkers et al. 1996; Pitiot et al. 1999).

Results

Using a variety of populations with imaging data collected in the same fashion, we have created a series of probabilistic atlases that retain information on anatomic and functional variability (Mazziotta et al. 1995; Thompson et al. 1997). Descriptions of several of these follow. As the subject database increases in size and content, the digital form of these atlases allows efficient statistical comparisons of individuals or groups. In addition, the population that an atlas represents can be stratified into subpopulations to represent specific disease types, and subsequently by age, gender, handedness, or genetic factors.

Pathology detection

Normal anatomic complexity makes it difficult to design automated strategies that detect abnormal brain structure. At the same time, brain structure is so variable that group-specific patterns of anatomy and function are often obscured. Reports of structural differences in the brain linked to gender, IQ, and handedness are a topic of intense controversy, and it is even less clear how these factors affect disease-specific abnormalities (Thompson and Toga 1999). The importance of these linkages has propelled computational anatomy to the forefront of brain imaging investigations. To distinguish abnormalities from normal variants, a realistically complex mathematical framework is required to encode information on anatomic variability in homogeneous populations (Grenander and Miller 1998). We employed elastic registration or *warping* algorithms to achieve distinct advantages for encoding patterns of anatomic variation and detecting pathology. Cortical patterns are altered in schizophrenia (Narr et al. 2000), Alzheimer's Disease (Thompson et al. 1998, 2000c) and a wide variety of developmental disorders. By using specialized strategies for group averaging of anatomy, specific features of anatomy emerge which are not observed in individual representations due to their considerable variability. Group-specific patterns of cortical organization or asymmetry can then be mapped out and visualized (Thompson and Toga 1999; Narr et al. 1999).

Deformable probabilistic atlases

Warping algorithms create deformation maps (Fig. 2) that indicate 3D patterns of anatomic differences between any pair of subjects. By defining probability distributions on the space of deformation transformations that drive the anatomy of different subjects into correspondence (Thompson and Toga 1997), statistical parameters of these distributions can be estimated from databased anatomic data to determine the magnitude and directional biases of anatomic variation. Encoding of local variation can then be used to assess the severity of structural variants outside of the normal range, which, in brain data, may be a sign of disease (Thompson et al. 1997).

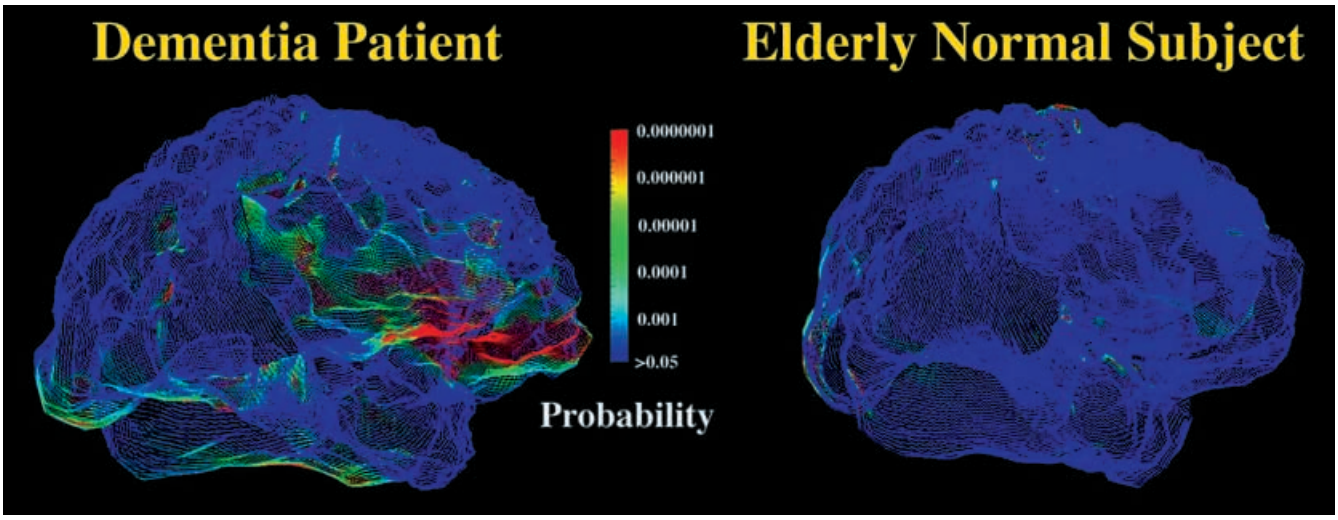

Fig. 3 Pathology detection in Alzheimer's disease. A color-coded probability map (left), shown on a 3D graphical surface model of an Alzheimer's patient's cortex, provides probability statements about the deviation of cortical regions from the norm. The inherent variability in normal cortical anatomy is encoded in the form of a surface-based probability field, known as an anisotropic lattice process, or a random vector field. The resulting map exhibits regions of severely depressed probability values ($P<0.00001$), particularly in inferior frontal cortex. A probability map is also shown (right) for a normal control subject. The system is refined as the underlying database of subjects increases in size and content. (Adapted from Thompson et al. 1997)

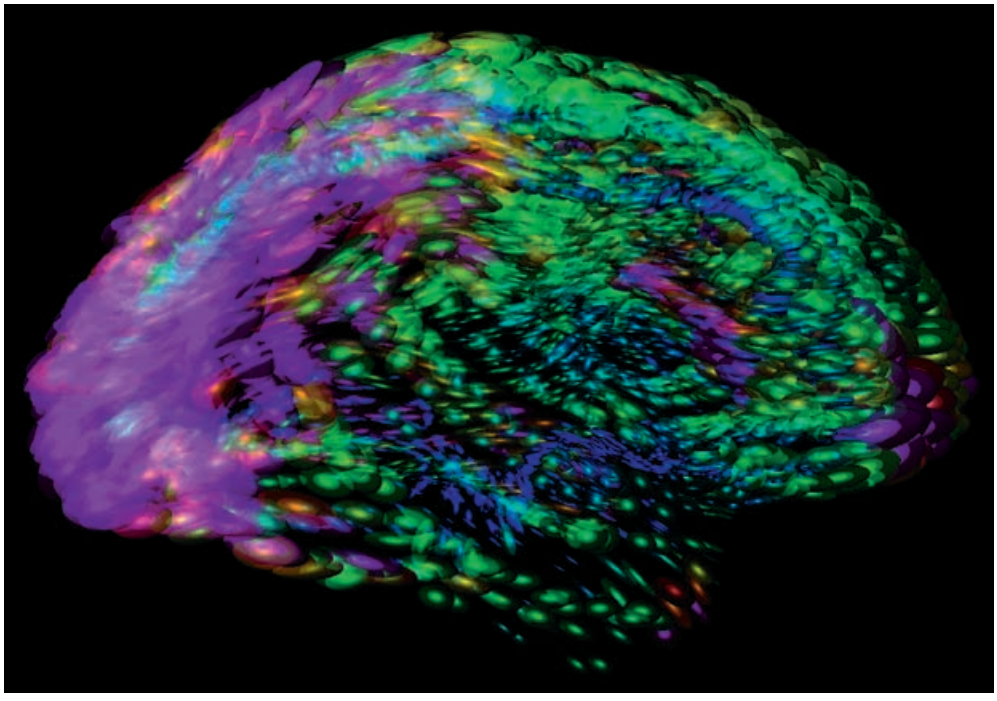

Fig. 4 Tensor maps reveal directional biases in normal cortical variability yielding probabilistic confidence limits on normal anatomic variation ($n=20$). Tensor maps can be used to visualize complex patterns of gyral pattern variation at the cortex. The maps are based on the group of 20 elderly normal subjects. Color distinguishes regions of high variability (*pink colors*) from areas of low variability (*blue*). Ellipsoidal glyphs indicate the principal directions of variation – they are most elongated along directions where there is greatest anatomic variation across subjects. Each glyph represents the covariance tensor of the vector fields that map individual subjects onto their group average anatomic representation. Variability is greatest in temporo-parietal cortex. Since cortical variations are modeled as vector field displacements of an average cortical model, ellipsoids of constant probability density can be computed for specific gyral and sulcal regions (relative to an average cortex). These probability fields are obtained by singular value decomposition, or Cholesky factorization, of the local covariance tensor (Thompson et al. 1996a). Confidence ellipsoids are shown, colored by the determinant of the covariance tensor, which measures the magnitude of anatomic variability at each location. (Adapted from Thompson et al. 2000c)

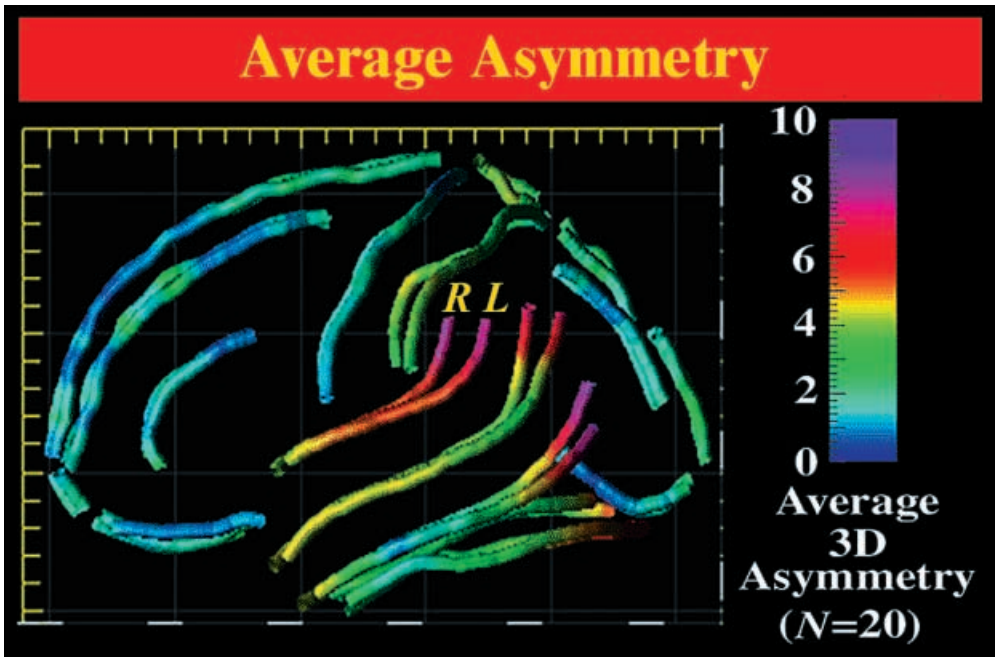

Fig. 5 Population-based maps of cortical pattern asymmetry. Averaging of cortical patterns across subjects (N=20, normal subjects) reveals fundamental features in the profile of asymmetry across the normal human cortex. Asymmetry is measured by globally mapping all brains into a standard 3D space with the average size and shape for the group. Curves representing elements of the gyral pattern are averaged together across subjects, and these averaged models can be reflected in the interhemispheric plane for comparison with their homologues in the opposite brain hemisphere. The asymmetry shown locally is the amount of deformation required, in mm, to match points on one curve with corresponding points on the reflected contralateral curve. Highest asymmetry is found at the posterior limits of the Sylvian fissures, which overly language cortices that are structurally and functionally different in each brain hemisphere. The marked shape asymmetries in the gyral patterns of the temporo-parietal cortices and the postcentral sulci are clearly apparent, and their average magnitude can be charted in a population. Based on the average models for each cortical sulcus, asymmetry can be quantified locally, in 3D, revealing general trends not apparent in the cortical anatomy of an individual. (Adapted from Thompson et al. 2000b)

Encoding brain variation

To see if disease-specific features could be detected in individual patients, we developed a *random vector field* approach to construct a population-based brain atlas (Thompson and Toga 1997). Briefly, given a 3D MR image of a new subject, a warping algorithm calculates a set of high-dimensional volumetric maps, elastically matching this image with other scans from an anatomic image database. Target scans are selected from subjects matched for age, handedness, gender, and other demographic factors (Thompson et al. 1997, 1998). The resulting family of volumetric warps provides empirical information on local variability patterns. A probability space of random transformations, based on the theory of anisotropic Gaussian random fields (Thompson et al. 1997), with statistical flattening corrections (Worsley et al. 1999; Thompson et al. 2000b) is then used to encode the variations. For the cortex, specialized approaches are needed to represent variations in gyral patterns (Thompson et al. 1997; Thompson and Toga 1998). Confidence limits in stereotaxic space are determined, for points in the new subject's brain, enabling the creation of probability maps to highlight and quantify regional patterns of deformity (Fig. 3).

Fig. 4 shows a tensor map of variability for normal subjects, after mapping 20 elderly subjects' data into Talairach space (all right handed, 10 males, 10 females). Ellipsoidal glyphs indicate the principal directions of variation – they are most elongated along directions where anatomic variation is greatest across subjects. Each glyph represents the covariance tensor of the vector fields that map individual subjects onto their group average. Because gyral patterns constrain the mappings, the fields reflect variations in cortical organization at a more local level than can be achieved by only matching global cortical geometry. Note the elongated glyphs in anterior temporal cortex, and the very low variability (in any direction) in entorhinal and inferior frontal areas. By better defining the parameters of allowable normal variations, the resulting information can be leveraged to distinguish normal from abnormal anatomical variants.

Brain asymmetry

A feature observable from the average anatomical models is that consistent patterns of brain asymmetry can be mapped, despite wide variations in asymmetry in individual subjects (Fig. 5). In dementia, the increased cortical asymmetry probably reflects asymmetric progression of the disease. Fig. 6 shows average maps of the lateral ventricles, again from Alzheimer's disease and matched

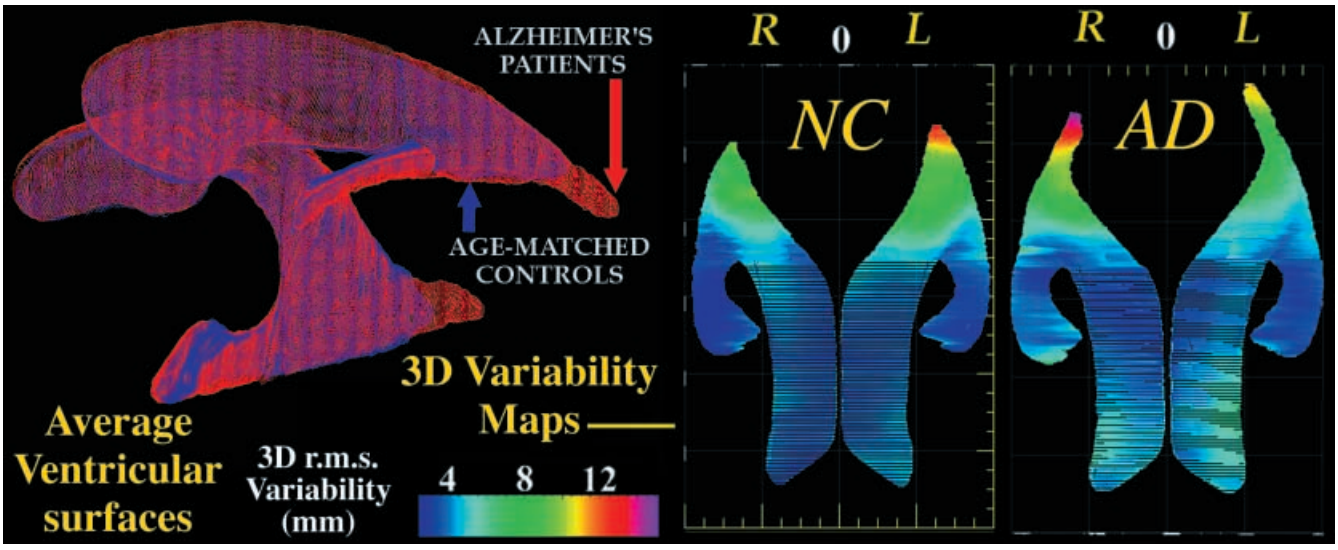

Fig. 6 Population-based maps of average ventricular anatomy in normal aging and Alzheimer's disease. In patients and controls, 3D parametric surface meshes (Thompson et al. 1996a) were used to model 14 ventricular elements, and meshes representing each surface element were averaged by hemisphere in each group. An average model for Alzheimer's patients (*red;* AD) is superimposed on an average model for matched normal controls (*blue; NC*). Mesh averaging reveals enlarged occipital horns in the Alzheimer's patients, and high stereotaxic variability in both groups. Extreme variability at the occipital horn tips also contrasts sharply with the stability of septal and temporal ventricular regions. A top view of these averaged surface meshes reveals localized asymmetry, variability, and displacement within and between groups. These subcortical asymmetries emerge only after averaging of anatomical maps in large groups of subjects. (Adapted from Thompson et al. 2000c)

elderly normal populations. As expected, the ventricles are significantly enlarged in dementia. Notice, however, that a pronounced asymmetry is observed in both groups (left volume larger than right, $P< 0.05$). This is an example of an effect that becomes clear after group averaging of anatomy, and is not universally apparent in individual subjects. It is, however, consistent with prior volumetric measurements (Shenton et al. 1992; Aso et al. 1995). Anatomical averaging can also be cross-validated with a traditional volumetric approach. Occipital horns were on average 17.1% larger on the left in the normal group (4070.1±479.9 mm^3) than on the right (3475.3± 334.0 mm^3; $P< 0.05$), but no significant asymmetry was found for the superior horns (left: 8658.0±976.7 mm^3; right: 8086.4±1068.2 mm^3; $P>0.19$) or for the inferior horns (left: 620.6±102.6 mm^3; right: 573.7±85.2 mm^3; $P>0.37$). The asymmetry is clearly localized in the 3D group average anatomic representations. In particular, the occipital horn extends (on average) 5.1 mm more posteriorly on the left than the right. The capacity to resolve asymmetries in a group atlas can assist in studies of disease-specific cortical organization (Thompson et al. 1997, 2000a,b; Mega et al. 1998; Zoumalan et al. 1999; Narr et al. 1998, 1999, 2000).

To see if cortical asymmetries were lost in schizophrenia, we made average cortical representations for schizophrenic patients (n=25; 15 males, 10 females; all right-handed) and matched controls (n=28; 15 males, 13 females). As described in the Methods section, thirty-six major sulcal curves were used to drive each subject's gyral pattern into a group mean configuration (Fig. 7). The magnitude of anatomic variation in each brain region was also computed from the deformation vector fields, and shown in color as a variability map. Perhaps surprisingly, asymmetry was not attenuated in the patient group. Marked asymmetries were observed in the sagittal projections of average anatomy for each group. Significant asymmetries were confirmed by calculating curvature and extent measures from the parametric mesh models (Narr et al. 1999). In frontal cortex, the patients also displayed greater variability than controls.

Corpus callosum differences

We also attempted to identify regionally selective patterns of callosal change in patient groups with Alzheimer's disease and schizophrenia (Thompson et al. 1998; Narr et al. 1999). The mid-sagittal callosum was first partitioned into 5 sectors (Duara et al. 1991; Larsen et al. 1992). This roughly segregates callosal fibers from distinct cortical regions. In AD, focal fiber loss was expected at the callosal isthmus (sector 2) whose fibers selectively innervate the temporo-parietal regions with early neuronal loss and perfusion deficits (Brun and Englund 1981). Consistent with this hypothesis, a significant area reduction at the isthmus was found, reflecting a dramatic 24.5% decrease from 98.0± 8.6 mm^2 in controls to 74.0±5.3 mm^2 in AD ($P< 0.025$). Terminal sectors (1 and 5) were not significantly atrophied, and the central midbody sector showed only a trend toward significance (16.6% mean area loss; $P< 0.1$), due to substantial inter-group overlap. Average boundary representations, however, localized these findings directly (cf. Fig. 8).

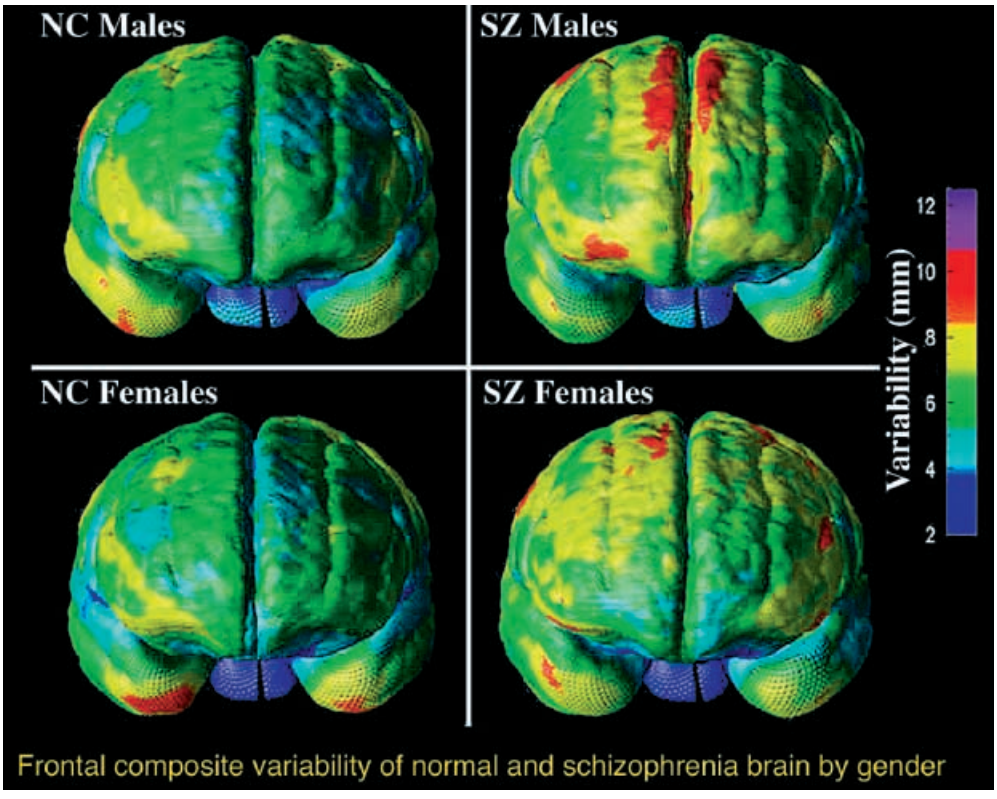

Fig. 7 Profiles of anatomical variability across the cortex in schizophrenia. In schizophrenia, there is a region of greater anatomical variability in frontal cortex, which is found in both male and female patients (*SZ*) but not in normal controls (*NC*). In diseases such as schizophrenia (Narr et al. 2000) and Alzheimer's disease (Thompson et al. 1998), anatomical variability may be increased, and normal variations may be compounded by additional pathologic change. (Data from Narr et al. 2000)

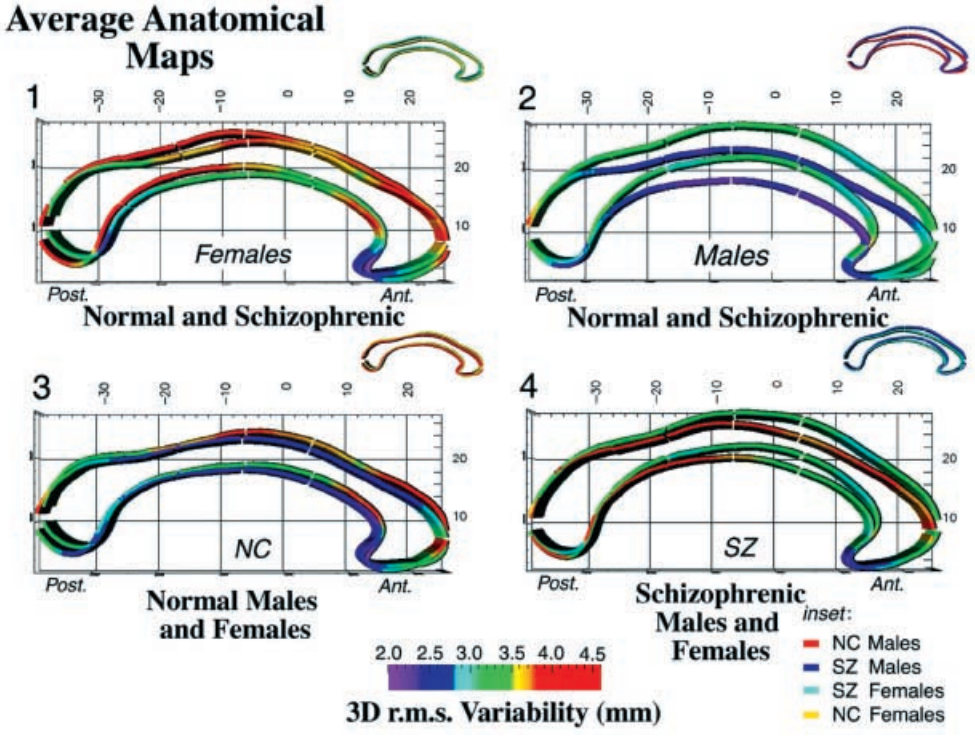

Fig. 8 1–4 Average corpus callosum shapes in schizophrenia. Midsagittal corpus callosum boundaries were averaged from 25 patients with chronic schizophrenia (DSM-III-R criteria; 15 males, 10 females; age: 31.1 +/– 5.6 yrs.) and from 28 control subjects matched for age (30.5 +/– 8.7 yrs.), gender (15 males, 13 females) and handedness (1 left-handed subject per group). Profiles of anatomic variability around the group averages are also shown (*in color*) as an r.m.s. deviation from the mean. Anatomical averaging reveals a pronounced and significant bowing effect in the schizophrenic patients relative to normal controls. Male patients show a significant increase in curvature for superior and inferior callosal boundaries ($P < 0.001$), with a highly significant sex by diagnosis interaction ($P < 0.004$). The sample was stratified by sex and diagnosis and separate group averages show that the disease induces less bowing in females (**1**) than in males (**2**). While gender differences are not apparent in controls (**3**), a clear gender difference is seen in the schizophrenic patients (**4**). Abnormalities localized in a disease-specific atlas can therefore be analyzed to reveal interactions between disease and demographic parameters. (Data from Narr et al. 2000)

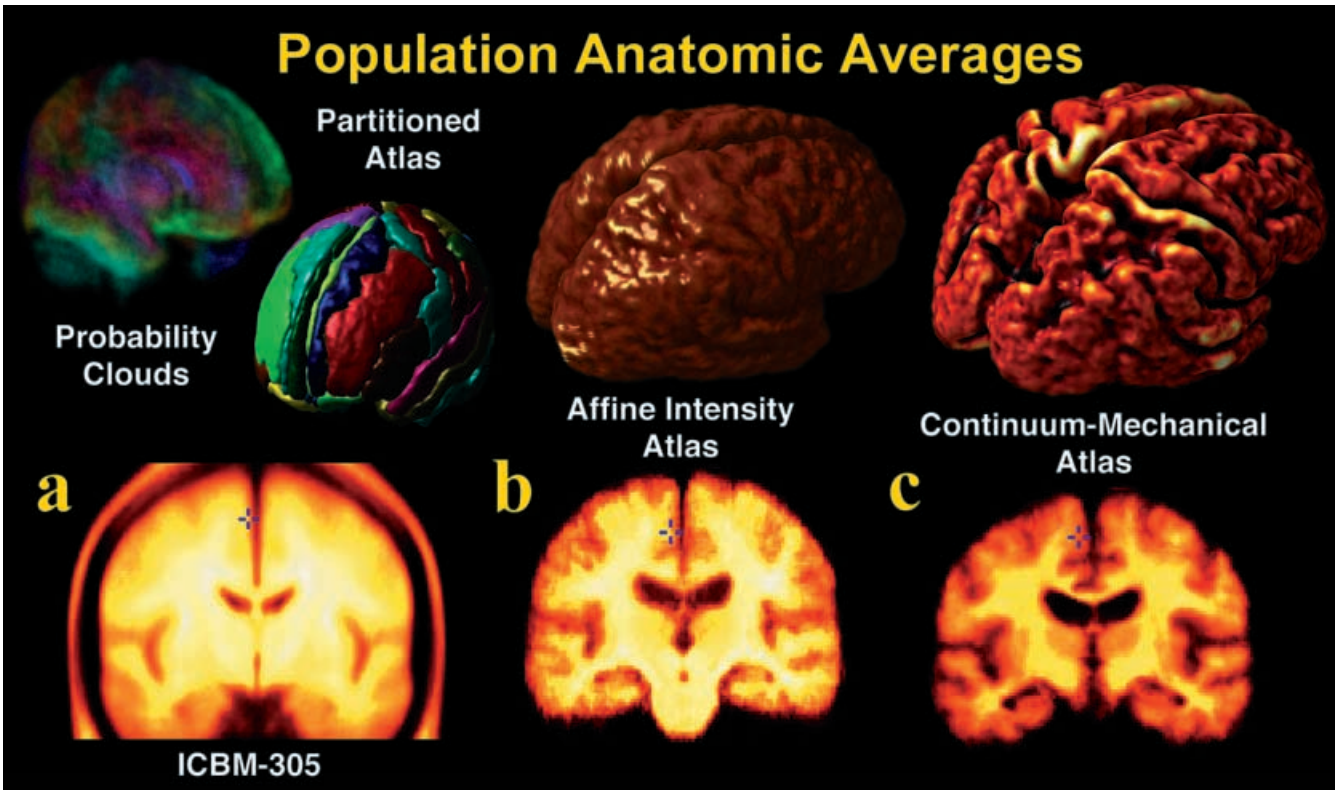

Fig. 9a–c Average brain templates. **a** In a widely-used average brain image template (ICBM305) based on voxel-wise intensity averaging of 305 young normal subjects' scans (Evans et al. 1994), anatomical features are not well-resolved at the cortex. Cortical variability is represented using probability clouds (*top left*) that describe the frequency of incidence for each gyrus at each stereotaxic voxel, after linear registration and voxel-by-voxel comparison. In an affine brain template (**b**), similarly constructed from Alzheimer's disease patients' scans, the cortical average is also poorly resolved. By contrast, anatomical features are highly resolved, even at the cortex, in the *Continuum-mechanical brain template* (**c**), which applies a continuum-mechanical transformation to each brain before intensity averaging. Scans are elastically reconfigured into a group mean configuration, using surface-based warping to match 84 surface models (including gyral pattern elements) across all subjects. Reconfigured scans are then averaged voxel-by-voxel, after intensity normalization, to produce a group image template with the average geometry *and* average image intensity for the group. Vector field transformations of extremely high spatial dimension are required to resolve cortical features, in their mean configuration, after scans are averaged together (**c**). (Adapted from Thompson et al. 2000e)

Gender in schizophrenia

Different shape alterations were observed in schizophrenia (Narr et al. 1999). A significant bowing effect was observed, reflecting enlargement of the underlying 3rd ventricle. By creating separate average models for male and female patients, significant gender effects also emerged. The greater bowing effect in male than female patients was confirmed by multivariate analysis of variance, and is highlighted in the average anatomic templates. As emphasized by this example, even if no sex difference is present in normal callosal morphology (see Thompson et al. 2000d, for a review of this controversy), this does not preclude sex effects from interacting with morphometric abnormalities in diseased populations. In schizophrenia, there is typically a later age of onset in female schizophrenics, and hereditary factors may be unevenly distributed between the sexes (De Lisi et al. 1989; Waddington, 1993; Colombo et al. 1993). Stratification of probabilistic atlases by gender and other genetic factors provides a computationally fast way to visualize these effects and relate them to epidemiologic data (Mazziotta et al. 1995; Mega et al. 1998; Zoumalan et al. 1999; Blanton et al. 1999; Le Goualher et al. 1999).

Comparing a subject with an atlas

In one validation experiment (Thompson et al. 1997), probability maps were created to highlight abnormal deviations in the callosal and midline anatomy of a tumor patient. The two regions of metastatic tissue induced marked distortions in the normal architecture of the brain. After storing variations in deep surface anatomy as a spatially-adaptive covariance tensor field, probability maps were generated for the tumor patient. In the tumor patient, the herniation effects apparent in the blockface imagery were detected in the probability maps of structures near the lesion sites.

In one experiment mappings that deform one cortex into gyral correspondence with another were used to create an average cortex for patients with mild to moderate Alzheimer's disease (AD). Thirty-six gyral curves for 9 AD patients were transferred to the cortical parameter

space uniformly re-parameterized, and a set of 36 average gyral curves for the group was created by vector averaging of point locations on each curve. Each individual cortical pattern was then aligned with the average curve set using a spherical flow field. These 9 flow fields were then used to create an average cortex in 3D space, as follows. By carrying a code (that indexes 3D locations) along with the flow that aligns each individual with the average folding pattern, information can then be recovered at a particular location in the average folding pattern, specifying the 3D cortical points that map to it in each subject. By ruling a regular grid over the warped coded map, and reading off 3D position values for each subject, cortical positions in any subject's *original* 3D anatomy can be recovered. This produces a new coordinate grid on a given subject's cortex, in which particular grid-points appear in the same location relative to the primary gyral pattern across all subjects (see Fischl et al. 1999, for a similar approach). By averaging these 3D positions across subjects, an average 3D cortical model was constructed for the group (Fig. 9). The resulting mapping is guaranteed to average together all points falling on the same cortical locations across the set of brains, and ensures that corresponding cortical features are averaged together.

Discussion

The mathematical strategies employed in the construction of these atlases were needed to encode comprehensive information on structural variability in human populations. Particularly relevant is 3-dimensional statistical information on group-specific patterns of variation, and how these patterns are altered in disease. This information can be exploited by expert diagnostic systems, whose goal is to detect subtle or diffuse structural alterations in disease.

Pathology detection in image databases

Pattern recognition algorithms for automated identification of brain structures can also benefit greatly from encoded information on anatomic variability. We recently developed a Bayesian approach to identify the *corpus callosum* in each image in an MRI database (Pitiot et al. 1999). The shape of a deformable curve is progressively tuned to optimize a mathematical criterion measuring how likely it is that it has found the corpus callosum. The measure includes terms that reward contours based on their agreement with a diffused edge map, their geometric regularity, and their statistical abnormality when compared with a distribution of normal shapes. By averaging contours derived from an image database, structural abnormalities associated with Alzheimer's Disease and schizophrenia were identified (Thompson et al. 1998; Narr et al. 1999). Automated parameterization of structures will accelerate the identification and analysis of disease-specific structural patterns.

Disease progression

The atlases so far described, for the dementia and schizophrenia populations, have been based on homogeneous patient groups, matched for age, gender, handedness, and educational level. Since AD, in particular, is a progressive disease, the initial atlas was created to reflect a particular stage in the disease (MMSE score: 19.3±2.0). At this stage, patients often present for initial evaluation, and MR, PET and SPECT scans have maximal diagnostic value. Nonetheless, by expanding the underlying patient database, atlases are under construction to represent the more advanced stages of Alzheimer's disease. By stratifying the population according to different criteria, different atlases can be synthesized to represent other clinically defined groups.

4D Coordinate systems

Atlasing of data from the developing or degenerating brain presents unique challenges (Toga and Thompson 1998). However, warping algorithms can be applied to serial scan data to track disease and growth processes in their full spatial and temporal complexity. Maps of anatomical change can be generated by warping scans acquired from the same subject over time (Thirion and Calmon 1997; Thompson et al. 2000a). Serial scanning of human subjects (Fox et al. 1996; Freeborough et al. 1996; Subsol et al. 1997; Thompson et al. 1998) or experimental animals (Jacobs and Fraser 1994) in a dynamic state of disease or development offers the potential to create 4D models of brain structure. These models incorporate dynamic descriptors of how the brain changes during maturation or disease. They are therefore of interest for investigating and staging brain development. In an atlas setting, these 4-dimensional maps can act as normative data to define aberrant growth rates and their modulation by therapy (Haney et al. 2000a, b, c).

In our initial human studies (Thompson et al. 1998, 2000a), we developed several algorithms to create 4D quantitative maps of growth patterns in the developing human brain. Time-series of high-resolution pediatric MRI scans were analyzed. The resulting tensor maps of growth provided spatially-detailed information on local growth patterns, quantifying rates of tissue maturation, atrophy, shearing and dilation in the dynamically changing brain architecture. Pairs of scans were selected to determine patterns of structural change across the interscan interval. Deformation processes recovered by a high-dimensional warping algorithm were then analyzed using vector field operators to produce a variety of tensor maps. These maps were designed to reflect the magnitude and principal directions of dilation or contraction, the rate of strain, and the local curl, divergence and gradient of flow fields representing the growth processes recovered by the transformation.

The growth maps obtained in these studies exhibit several striking characteristics. First, foci of rapid

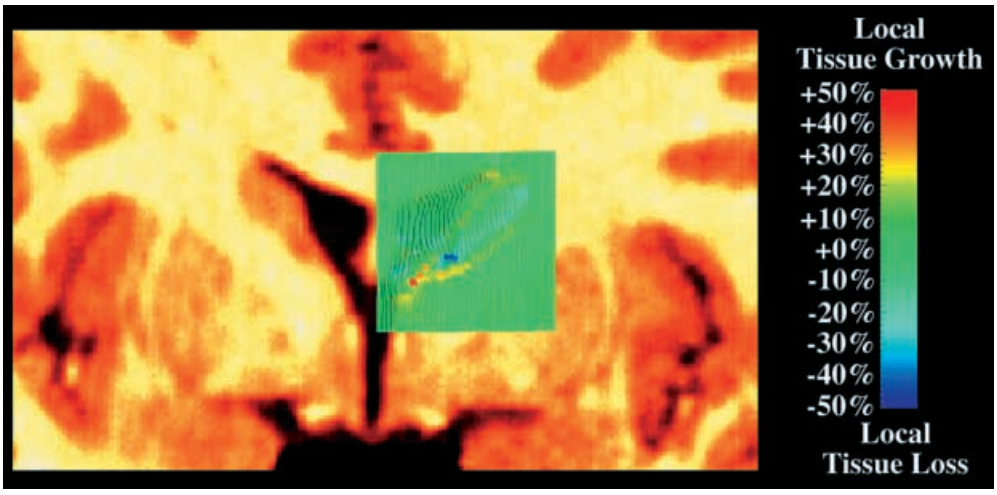

Fig. 10 Patterns of deep nuclear tissue loss. In the 4-year period from 7 to 11 years of age, a young normal male subject exhibits a local 50% tissue *loss* at the caudate head, as well as a 20–30% growth of the internal capsule and a 5–10% dilation of the superior ventricular horn (Thompson et al. 2000a). Graphical visualizations of growth rates indicate the regional complexity of the growth processes between the two scans. (Adapted from Thompson et al. 2000a)

growth at the callosal isthmus appeared consistently across puberty. These rates appeared to attenuate as subjects progressed into adolescence (Thompson et al. 2000a). Rapid rates of tissue loss were also revealed at the head of the caudate, in an earlier phase of development (Fig. 10).

In the near future, 4D atlases will be able to map growth and degeneration in their full spatial and temporal complexity. Despite the logistic and technical challenges, these mapping approaches hold tremendous promise in analyzing the dynamics of degenerative or neoplastic diseases (Haney et al. 2000a,b,c). They will ultimately play a role in detecting how different therapeutic approaches modulate the course of disease.

Multi-modality atlases

Combining data derived from multiple subjects with data from multiple modalities enable can result in comprehensive representations of structure/function relationships and help elucidate subtle results difficult to appreciate in isolation. In the construction of anatomic atlases, the in vivo resolution available from MR is incapable of characterizing the cytoarchitectural detail available from post mortem material. Because of the superior anatomic resolution, several digital atlases have been created using cryosection imaging. This technique allows the serial collection of photographic images from a cryoplaned specimen blockface (Bohm et al. 1983; Greitz et al. 1991; Toga et al. 1994). Using 1024^2, 24-bits/pixel digital color cameras, cryosection imaging offers a spatial resolution as high as 100 microns/voxel for whole human head cadaver preparations, or higher for isolated brain regions (Toga et al. 1997). In the *Visible Human Project* (Spitzer et al. 1996), two (male and female) cadavers were cryoplaned and imaged at 1.0 mm intervals (0.33 mm for the female data), and the entire bodies were also reconstructed via 5,000 post mortem CT and MRI images. The resulting digital datasets consist of over 15 gigabytes of image data. While not an atlas per se, the *Visible Human* data has served as the foundation for developing related atlases of regions of the cerebral cortex (Drury and Van Essen 1997), and high-quality brain models and visualizations (Schiemann et al. 1996; Stewart et al. 1996). Using multi-modality data from a patient with a localized pathology, and more recently the *Visible Human* data, Höhne and co-workers developed a commercially available brain atlas designed for teaching neuroanatomy (VOXEL-MAN; Höhne et al. 1990, 1992; Tiede et al. 1993; Pommert et al. 1994).

Using 1024^2, 24-bits/pixel digital color cameras, spatial resolution can be as high as 50 microns/voxel for whole human head cadaver preparations, or higher for isolated brain regions (Toga et al. 1994). Cryosectioning in micron increments permits data collection with high spatial resolution in the axis orthogonal to the sectioning plane.

Integration of metabolic and functional images acquired in vivo with post mortem biochemical maps provides a unique view of the relationship between brain function and pathology. Mega et al. (1997) scanned Alzheimer's patients in the terminal stages of their disease using both MRI and PET. Using elastic registration techniques (Thompson et al. 1996a), these data were combined with *post mortem* histologic images showing the gross anatomy (Toga et al. 1994), a Gallyas stain of neurofibrillary tangles, and a variety of spatially indexed biochemical assays. The resulting multimodality maps of the Alzheimer's disease brain relate the anatomic and histopathologic underpinnings of the disease in a standardized coordinate space. These data are further correlated with in vivo metabolic and perfusion maps of this disease. The resulting maps are key components of a growing disease-specific atlas (Mega et al. 2000).

Conclusion

The uses of brain atlases are as varied as their construction. They provide the ability to measure, visualize, compare and summarize brain images. They encompass de-

scriptions of structure or function of the whole brain to maps of groups or populations. Individual systems of the brain can be mapped as can changes over time, as in development or degeneration. An atlas enables comparison across individuals, modalities or states. But in most cases, the value added by brain atlases is the unique and critical ability to integrate information from multiple sources. The utility of an atlas is dependent upon appropriate coordinate systems, registration and deformation methods along with useful visualization strategies. The probabilistic systems described here show promise for encoding patterns of anatomic variation in large image databases, for pathology detection in individuals and groups, and for determining effects in space and time on brain structure of age, gender, handedness and other demographic or genetic factors.

Acknowledgments This work was supported by research grants from the National Center for Research Resources (P41 RR13642 and RR05956), the National Institute of Neurological Disorders and Stroke and the National Institute of Mental Health (NINDS/NIMH NS38753), and by a Human Brain Project grant to the International Consortium for Brain Mapping, funded jointly by NIMH and NIDA (P20 MH/DA52176). Additional support was also provided by the National Library of Medicine (LM/MH05639) and National Science Foundation (BIR 93-22434).

References

Ashburner J, Neelin P, Collins DL, Evans AC, Friston KJ (1997) Incorporating prior knowledge into image registration, Neuroimage 6:344–352

Aso M, Kurachi M, Suzuki M, Yuasa S, Matsui M, Saitoh O (1995) Asymmetry of the ventricle and age at the onset of schizophrenia. Eur Arch Psychiatry Clin Neurosci 245:142–144

Avoli M, Hwa GC, Kostopoulos G, Oliver A, Villemure JG (1991) Electrophysiological analysis of human neocortex in vitro: experimental techniques and methodological approaches, Can J Neurol Sci 18:636–639.

Berger H (1929) Uber das Elektrenkephalogramm des Menschen. Arch Psychiatr Nervenkr 87:527–580

Blanton RE, Levitt J, Thompson PM, Badrtalei S, Capetillo-Cunliffe L, Toga AW (1999) Average 3-dimensional caudate surface representations in a juvenile-onset schizophrenia and normal pediatric population. Presentation 621, 5th International Conference on Functional Mapping of the Human Brain, Dusseldorf, Germany, June 1999

Bohm C, Greitz T, Kingsley D, Berggren BM, Olsson L (1983) Adjustable computerized brain atlas for transmission and emission tomography. Am J Neuroradiol 4:731–733

Brodmann K (1909). Vergleichende Lokalisationslehre der Grosshirnrinde in ihren Prinzipien dargestellt auf Grund des Zellenbaues, Barth, Leipzig, In: Some papers on the cerebral cortex, translated as: on the comparative localization of the cortex, 201–230, Thomas, Springfield, Il, 1960

Bro-Nielsen M, Gramkow C (1996) Fast fluid registration of medical images, In: Höhne KH, Kikinis R (eds) Visualization in biomedical computing, Hamburg, Germany. Lecture notes in computer science 1131:267–276. Springer, Berlin Heidelberg New York

Brun A, Englund E (1981) Regional pattern of degeneration in Alzheimer's disease: neuronal loss and histopathologic grading, Histopathology 5:549–564

Burke HL, Yeo RA, Delaney HD, Conner L (1993) CT scan cerebral hemispheric asymmetries: predictors of recovery from aphasia. J Clin Exp Neuropsychol 15(2): 191–204

Christensen GE, Rabbitt RD, Miller MI (1993) A deformable neuroanatomy textbook based on viscous fluid mechanics. 27th Ann. Conf. on Information Sciences and Systems, pp 211–216

Christensen GE, Rabbitt RD, Miller MI (1996) Deformable templates using large deformation kinematics, IEEE Trans. on Image Processing, Oct. 1996, 5:1435–1447

Collins DL, Neelin P, Peters TM, Evans AC (1994a) Automatic 3D intersubject registration of MR volumetric data into standardized Talairach space, J. Comp. Assisted Tomography, 18:192–205

Collins DL, Peters TM, Evans AC (1994b) An automated 3D nonlinear image deformation procedure for determination of gross morphometric variability in the human brain. Proc Visualization Biomed Comp (SPIE) 3:180–190

Colombo C, Bonfanti A, Livian S, Abbruzzese M, Scarone S (1993) Size of the corpus callosum and auditory comprehension in schizophrenics and normal controls. Schizophr Res:1:63–70

Damasio H (1995) Human brain anatomy in computerized images. Oxford University Press, Oxford New York

Davatzikos C (1996) Spatial normalization of 3D brain images using deformable models, J Comp Assisted Tomography 20: 656–665

DeLisi LE, Dauphinais ID, Hauser P (1989) Gender differences in the brain: are they relevant to the pathogenesis of schizophrenia? Comp Psychiatry 30:197–208

Dinov ID, Thompson PM, Woods RP, Mega MS, Holmes CJ, Sumners D, Saxena S, Toga AW (1999) Probabilistic sub-volume partitioning techniques for determining the statistically significant regions of activation in stereotaxic functional data. J Comp Assisted Tomography 24(1): 128–138

Drury HA, Essen DC van (1997) Analysis of functional specialization in human cerebral cortex using the visible man surface based atlas. Hum Brain Mapping 5:233–237

Drury HA, Essen DC van, Joshi SC, Miller MI (1996) Analysis and comparison of areal partitioning schemes using two-dimensional fluid deformations. Poster presentation, 2nd Int. Conf. on Functional Mapping of the Human Brain, Boston, Massachusetts USA, June 17–21 1996, NeuroImage 3:S130

Duara R, Kushch A, Gross-Glenn K, Barker WW, Jallad B, Pascal S, Loewenstein DA, Sheldon J, Rabin M, Levin B (1991) Neuroanatomic differences between dyslexic and normal readers on magnetic resonance imaging scans, Arch Neurol 48:410–416

Duvernoy HM (1991) The human brain, Springer, New York Heidelberg Berlin

Evans AC, Dai W, Collins DL, Neelin P, Marrett S (1991) Warping of a computerized 3D atlas to match brain image volumes for quantitative neuroanatomical and functional analysis, SPIE Med. Imaging 1445:236–247

Evans AC, Collins DL, Neelin P, MacDonald D, Kamber M, Marrett TS (1994) Three-dimensional correlative imaging: applications in human brain mapping, In: (eds) Functional neuroimaging: technical foundations, Thatcher RW, Hallett M, Zeffiro T, John ER, Huerta M, 145–162

Evans AC, Collins DL, Milner B (1992) An MRI-based stereotactic brain atlas from 300 young normal subjects, Proceedings of the 22nd Symposium of the Society for Neuroscience, Anaheim, 408

Fischl B, Sereno MI, Tootell RBH, Dale AM (1999) High-resolution inter-subject averaging and a co-ordinate system for the cortical surface, Hum Brain Mapping 8(4): 272–284

Fox NC, Freeborough PA, Rossor MN (1996) Visualization and quantification of rates of cerebral atrophy in Alzheimer's disease. Lancet 348(9020):94–97

Fox PT, Perlmutter JS, Raichle M (1985) A stereotactic method of localization for positron emission tomography. J Comput Assist Tomogr 9:141–153

Fox PT, Mintun MA, Reiman EM, Raichle ME (1988) Enhanced detection of focal brain responses using inter-subject averaging and change distribution analysis of subtracted PET images. J Cereb Blood Flow Metab 8:642–653

Freeborough PA, Woods RP, Fox NC (1996) Accurate registration of serial 3D MR brain images and its application to visualizing change in neurodegenerative disorders. J Comput Assist Tomogr 20:1012–1022

Friston KJ, Passingham RE, Nutt JG, Heather JD, Sawle GV, Frackowiak RSJ (1989) Localization in PET images: direct fitting of the intercommissural (AC-PC) line. J Cereb Blood Flow Metab 9:690–695

Friston KJ, Frith CD, Liddle PF, Frackowiak RSJ (1991) Plastic transformation of PET images. J Comp Assist Tomogr 9:141–153

Friston KJ, Holmes AP, Worsley KJ, Poline JP, Frith CD, Frackowiak RSJ (1995) Statistical parametric maps in functional imaging: a general linear approach. Hum Brain Mapping 2:189–210

Gee JC, Bajscy RK (1998) Elastic matching: continuum-mechanical and probabilistic analysis. In: Toga AW (ed) Brain warping. Academic Press, San Diego

Gee JC, Reivich M, Bajcsy R (1993) Elastically deforming an atlas to match anatomical brain images. J Comput Assist Tomogr 17:225–236

Greitz T, Bohm C, Holte S, Eriksson L (1991) A computerized brain atlas: construction, anatomical content and application. J Comput Assist Tomogr 15:26–38

Grenander U, Miller MI (1998) Computational anatomy: an emerging discipline. Technical report, Department of Mathematics, Brown University

Haller JW, Banerjee A, Christensen GE, Gado M, Joshi S, Miller MI, Sheline Y, Vannier MW, Csernansky JG (1997) Three-dimensional hippocampal MR morphometry with high-dimensional transformation of a neuroanatomic atlas. Radiology 202:504–510

Haney S, Thompson PM, Cloughesy TF, Alger JR, Frew A, Toga AW (2000a) Cross-validation of tissue classification and surface modeling algorithms for determining growth rates of malignant gliomas: prognostic value of growth rates and MR spectroscopy, The 2000 International Conference on Mathematics and Engineering Techniques in Medicine and Biological Sciences, Las Vegas, June 2000

Haney S, Thompson PM, Cloughesy TF, Alger JR, Frew A, Toga AW (2000b) Prognostic value of growth rates and spectroscopic data in patients with malignant gliomas, Proc Soc Neurosci

Haney S, Thompson PM, Cloughesy TF, Alger JR, Toga AW (2000c) Tracking tumor growth rates in patients with malignant gliomas: a test of two algorithms. Am J Neuroradiol 22(1): 73–82

Höhne KH, Bomans M, Pommert A, Riemer M, Schiers C, Tiede U, Wiebecke G (1990) 3D visualization of tomographic volume data using the generalized voxel model. Visual Comput 6:28–36

Höhne KH, Bomans M, Riemer M, Schubert R, Tiede U, Lierse W (1992) A 3D anatomical atlas based on a volume model, IEEE Comput Graphics Appl 12:72–78

Holman LB, Chandak PK, Garada BM (1994) Atlas of brain perfusion SPECT, http://brighamrad.harvard.edu/education/online/BrainSPECT/BrSPECT.html

Holmes CJ, Hoge R, Collins L, Woods R, Toga AW, Evans AC (1998) Enhancement of MR images using registration for signal averaging. J Comput Assist Tomogr 22:324–333

Jacobs RE, Fraser SE (1994) Magnetic resonance microscopy of embryonic cell lineages and movements. Science 263(5147): 681–684

Kikinis R, Shenton ME, Iosifescu DV, McCarley RW, Saiviroonporn P, Hokama HH, Robatino A, Metcalf D, Wible CG, Portas CM, Donnino R, Jolesz F (1996) A digital brain atlas for surgical planning, model-driven segmentation, and teaching, IEEE Trans. on Visualization and Comput Graphics 2:232–241

Larsen JP, Høien T, Ödegaard H (1992) Magnetic resonance imaging of the corpus callosum in developmental dyslexia, Cognitive Neuropsychol 9:123–134

Le Bihan D (1996) Functional MRI of the brain: principles, applications and limitations. Neuroradiol 23:1–5

Le Goualher G, Procyk E, Collins DL, Venugopal R, Barillot C, Evans AC (1999) Automated extraction and variability analysis of sulcal neuroanatomy, IEEE Trans Med Imaging 18:206–217

Lehmann ED, Hawkes D, Hill D, Bird C, Robinson G, Colchester A, Maisley M (1991) Computer-aided interpretation of SPECT images of the brain using an MRI-derived neuroanatomic atlas. Med Informatics 16:151–166

MacDonald D (1998) A method for identifying geometrically simple surfaces from three dimensional images. PhD Thesis, McGill University, Canada

Mangin J-F, Frouin V, Bloch I, Regis J, Lopez-Krahe J (1994) Automatic construction of an attributed relational graph representing the cortex topography using homotopic transformations. SPIE 2299:110–121

Mansour A, Fox CA, Burke S, Akil H, Watson SJ (1995) Immunohistochemical localization of the cloned Mu Opioid receptor in the rat CNS. J Chem Neuroanat 8:283–305

Matsui T, Hirano A (1978) An atlas of the human brain for computerized tomography. Igako-Shoin

Mazziotta JC, Toga AW, Evans AC, Fox P, Lancaster J (1995) A probabilistic atlas of the human brain: theory and rationale for its development. NeuroImage 2: 89–101

Mega MS, Chen S, Thompson PM, Woods RP, Karaca TJ, Tiwari A, Vinters H, Small GW, Toga AW (1997) Mapping pathology to metabolism: coregistration of stained whole brain sections to PET in Alzheimer's disease. NeuroImage 5:147–153

Mega MS, Thompson PM, Cummings JL, Back CL, Xu LQ, Zohoori S, Goldkorn A, Moussai J, Fairbanks L, Small GW, Toga AW (1998) Sulcal variability in the Alzheimer's brain: correlations with cognition. Neurology 50:145–151

Mega MS, Chu T, Mazziotta JC, Trivedi KH, Thompson PM, Shah A, Cole G, Frautschy SA, Toga AW (1999) Mapping biochemistry to metabolism: FDG-PET and beta-amyloid burden in Alzheimer's disease. NeuroReport 10:2911–2917

Mega MS, Thompson PM, Toga AW, Cummings JL (2000) Brain Mapping in Dementia. In: Toga AW, Mazziotta JC (eds) Brain mapping: the disorders. Academic Press, New York

Meltzer CC, Frost JJ (1994) Partial volume correction in emission-computed tomography: focus on Alzheimer disease. In: Thatcher RW, Hallett M, Zeffiro T, John ER, Huerta M (eds) Functional neuroimaging: technical foundations. Academic Press, pp 163–170

Minoshima S, Koeppe RA, Frey KA, Ishihara M, Kuhl DE (1994) Stereotactic PET atlas of the human brain: aid for visual interpretation of functional brain images. J Nucl Med 35:949–954

Narr KL, Cannestra AF, Thompson PM, Sharma T, Toga AW (1998) Morphological variability maps of the corpus callosum and fornix in schizophrenia, 4th Int Conf on Human Brain Mapping, NeuroImage 7:S506

Narr KL, Thompson PM, Sharma T, Moussai J, Cannestra AF, Toga AW (2000) Mapping corpus callosum morphology in schizophrenia. Cereb Cortex 10(1): 40–49

Narr KL, Thompson PM, Sharma T, Moussai J, Zoumalan CI, Wang W, Rayman J, Toga AW (1999) Cortical and subcortical asymmetries: sex effects in Schizophrenic and Normal Populations. Proc Soc Neurosci Miami

Narr KL, Thompson PM, Sharma T, Moussai J, Cannestra AF, Toga AW (2000) Mapping corpus callosum morphology in schizophrenia, Cereb Cortex 10(1):40–49

Ono M, Kubik S, Abernathey CD (1990) Atlas of the cerebral sulci. Thieme Stuttgart

Palovcik RA, Reid SA, Principe JC, Albuquerque A (1992) 3D Computer animation of electrophysiological responses. J Neurosci Methods 41:1–9

Paxinos G, Watson C (1986) The rat brain in stereotaxic coordinates. Academic Press, San Diego

Penfield W, Boldrey E (1937) Somatic motor and sensory representation in the cerebral cortex of man as studied by electrical stimulation. Brain 60:389–443

Pitiot A, Thompson PM, Toga AW (1999) Spatially and temporally adaptive elastic template matching. IEEE Transactions on Pattern Analysis and Machine Intelligence, 1999

Pommert A, Schubert R, Riemer M, Schiemann T, Tiede U, Höhne KH (1994) Symbolic modeling of human anatomy for visualization and simulation. IEEE Vis Biomed Comput 2359: 412–423

Rabbitt RD, Weiss JA, Christensen GE, Miller MI (1995) Mapping of hyperelastic deformable templates using the finite element method. Proc. SPIE 2573:252–265

Rizzo G, Gilardi MC, Prinster A, Grassi F, Scotti G, Cerutti S, Fazio F (1995) An elastic computerized brain atlas for the analysis of clinical PET/SPET data. Eur J Nucl Med 22:1313–1318

Roland PE, Zilles K (1994) Brain atlases – a new research tool. Trends Neurosci 17:458–467

Royackkers N, Desvignes M, Revenu M (1996) Construction automatique d'un atlas adaptatif des sillons corticaux, ORASIS 96, Clermont-Ferrand, pp. 187–192

Sandor SR, Leahy RM (1995) Towards automated labeling of the cerebral cortex using a deformable atlas. In: Bizais Y, Barillot C, Di Paola R (eds) Info Proc in Med Imag, June 1995, 127–138

Schaltenbrand G, Bailey P (1959) Introduction to stereotaxis with an atlas of the human brain. Thieme New York Stuttgart

Schaltenbrand G, Wahren W (1977) Atlas for Stereotaxy of the Human Brain, 2nd edn., Stuttgart: Thieme.

Schiemann T, Nuthmann J, Tiede U, Höhne KH (1996) Segmentation of the Visible Human for high-quality volume-based visualization. Vis Biomed Comput 4:13–22

Sereno MI, Dale AM, Liu A, Tootell RBH (1996) A surface-based coordinate system for a canonical cortex, Proc 2nd Int Conf Hum Brain Mapping. Boston. Neuroimage 3:S252

Shenton ME, Kikinis R, Jolesz FA, Pollack SD, LeMay M, Wible CG, Hokama H, Martin J, Metcalf D, Coleman M, McCarley R (1992) Abnormalities of the left temporal lobe and thought disorder in schizophrenia. N Engl J Med 327:9:604–612

Smith GE (1907) A new topographical survey of the human cerebral cortex, being an account of the distribution of the anatomically distinct cortical areas and their relationship to the cerebral sulci. J Anat 41:237–254

Spitzer V, Ackerman MJ, Scherzinger AL, Whitlock D (1996) The Visible Human male: a technical report. J Am Med Informatics Assoc 3:118–130. http://www.nlm.nih.gov/extramural_research.dir/visible_human.html

Stewart JE, Broaddus WC, Johnson JH (1996) Rebuilding the Visible Man. Vis Biomed Comput 4:81–86

Subsol G, Roberts N, Doran M, Thirion JP, Whitehouse GH (1997) Automatic Analysis of Cerebral Atrophy, Magn. Reson. Imaging, 15(8):917–927

Talairach J, Szikla G (1967) Atlas d'anatomie stereotaxique du telencephale: études anatomo-radiologiques. Masson & Cie Paris

Talairach J, Tournoux P (1988) Co-planar stereotaxic atlas of the human brain. Thieme New York

Thirion J-P (1995) Fast non-rigid matching of medical images. INRIA Internal Report 2547, Projet Epidaure, INRIA, France

Thirion J-P, Calmon G (1997) Deformation analysis to detect and quantify active lesions in 3D medical image sequences. INRIA Technical Report 3101

Thompson PM, Toga AW (1996) A surface-based technique for warping 3-dimensional images of the brain. IEEE Transactions on Medical Imaging 15:1–16

Thompson PM, Toga AW (1997) Detection, visualization and animation of abnormal anatomic structure with a deformable probabilistic brain atlas based on random vector field transformations. Medical Image Analysis 1:271–294

Thompson PM, Toga AW (1998) Anatomically-driven strategies for high-dimensional brain image warping and pathology detection. In: Toga AW (ed) Brain Warping, Academic Press, 311–336

Thompson PM, Toga AW (1998b) Mathematical/computational strategies for creating a probabilistic atlas of the human brain. Workshop on Statistics of Brain Mapping, Centre de Recherches Mathématiques, McGill University, Canada

Thompson PM, Toga AW (1999) Elastic image registration and pathology detection. In: Bankman I, Rangayyan R, Evans AC, Woods RP, Fishman E, Huang HK (eds) Handbook of Medical Image Processing, Academic Press, New York

Thompson PM, Schwartz C, Toga AW (1996a) High-resolution random mesh algorithms for creating a probabilistic 3D surface atlas of the human brain. NeuroImage 3:19–34

Thompson PM, Schwartz C, Lin RT, Khan AA, Toga AW (1996b) 3D statistical analysis of sulcal variability in the human brain. J Neurosci 16:4261–4274

Thompson PM, MacDonald D, Mega MS, Holmes CJ, Evans AC, Toga AW (1997) Detection and mapping of abnormal brain structure with a probabilistic atlas of cortical surfaces. J Comput Assist Tomogr 21:567–581

Thompson PM, Moussai J, Khan AA, Zohoori S, Goldkorn A, Mega MS, Small GW, Cummings JL, Toga AW (1998) Cortical variability and asymmetry in normal aging and Alzheimer's disease. Cereb Cortex 8:492–509

Thompson PM, Giedd JN, Woods RP, MacDonald D, Evans AC, Toga AW (2000a) Growth patterns in the developing brain detected by using continuum-mechanical tensor maps. Nature, 404:190–193

Thompson PM, Mega MS, Narr KL, Sowell ER, Blanton RE, Toga AW (2000b) Brain image analysis and atlas construction. In: Fitzpatrick M, Sonka M (ed) SPIE handbook on medical image analysis. Society of Photo-Optical Instrumentation Engineers (SPIE) Press, July 2000

Thompson PM, Mega MS, Toga AW (2000c) Disease-specific brain atlases. In: Toga AW, Mazziotta JC (eds). Brain mapping: the disorders. Academic Press, New York

Thompson PM, Narr KL, Blanton RE, Toga AW (2000d) Mapping structural alterations of the corpus callosum during brain development and degeneration. In: Iacoboni M, Zaidel E (eds) The corpus callosum. Kluwer Academic Press (in press)

Thompson PM, Woods RP, Mega MS, Toga AW (2000e) Mathematical/computational challenges in creating population-based brain atlases. Hum Brain Mapping 9:81–92

Thompson PM, Mega MS, Woods RP, Blanton RE, Moussai J, Zoumalan CI, Aron J, Cummings JL, Toga AW (2001) Cortical change in Alzheimer's disease detected with a disease-specific population-based brain atlas. Cereb Cortex 11:1–16

Tiede U, Bomans M, Höhne KH, Pommert A, Riemer M, Schiemann T, Schubert R, Lierse W (1993) A computerized 3D atlas of the human skull and brain. Am J Neuroradiol 14:551–559

Toga AW (1998) Brain Warping. Academic Press, New York

Toga AW, Mazziotta JC (1996) Brain mapping: the methods. Academic Press, San Diego

Toga AW, Thompson PM (1997) Measuring, mapping, and modeling brain structure and function. SPIE Medical Imaging Symposium, Feb. 1997, Newport Beach, Calif., USA; SPIE Lecture notes, vol 3033

Toga AW, Thompson PM (1998) Multimodal brain atlases. In: Medical image databases. Wong STC (ed) Kluwer Academic Press, pp 53–88

Toga AW, Ambach K, Quinn B, Hutchin M, Burton JS (1994) Postmortem anatomy from cryosectioned whole human brain. J Neurosci Methods 54:239–252

Toga AW, Goldkorn A, Ambach K, Chao K, Quinn BC, Yao P (1997) Postmortem cryosectioning as an anatomic reference for human brain mapping. Comput Med Imaging Graph 21: 131–41

Vaillant M, Davatzikos C (1999) Hierarchical matching of cortical features for deformable brain image registration. Proc Information Processing in Medical Imaging Budapest

Van Buren JM, Borke RC (1972) Variations and connections of the human thalamus, vols. 1 & 2. Springer, New York

Van Buren JM, Maccubin D (1962) An outline atlas of human basal ganglia and estimation of anatomic variants. J Neurosurg 19:811–839

Van Essen DC, Maunsell JHR (1983) Hierarchical Organization an Functional Streams in the Visual Cortex. Trends Neurol Sci 6:370–375

Van Essen DC, Drury HA, Joshi SC, Miller MI (1997) Comparisons between human and Macaque using shape-based deformation algorithms applied to cortical flat maps. 3rd Int Conference on Functional Mapping of the Human Brain, Copenhagen, May 19–23 1997, NeuroImage 5:S41

Waddington JL (1993) Neurodynamics of abnormalities in cerebral metabolism and structure in schizophrenia. Schizophr Bull 19:55–58

Warfield S, Dengler J, Zaers J, Guttmann CRG, Wells WM, Ettinger GJ, Hiller J, Kikinis R (1995) Automatic Identification of Gray Matter Structures form MRI to Improve the Segmentation of White Matter Lesions, Proc. Med. Robotics & Comp. Assist. Surg (MRCAS) pp 55–62

Woods RP (1996) Modeling for Intergroup Comparisons of Imaging Data, NeuroImage 4(3):84–94

Worsley KJ, Andermann M, Koulis T, MacDonald D, Evans AC (1999) Detecting changes in non-isotropic images, Hum Brain Mapping 8:98–101

Zhou Y, Thompson PM, Toga AW (1999) Automatic extraction and parametric representations of cortical sulci. Computer Graphics and Applications 19:49–55

Zijdenbos AP, Dawant BM (1994) Brain segmentation and white matter lesion detection in MR images. Crit Rev Biomed Eng 22:401–465

Zoumalan CI, Mega MS, Thompson PM, Fuh JL, Lindshield C, Toga AW (1999) Mapping 3D patterns of cortical variability in normal aging and Alzheimer's disease. Annual Conference of the American Academy of Neurology